Separating annual, interannual and regional change in Sea Surface Temperature in the Northeastern Atlantic and Nordic Seas

Saes, Mischa J. M.; Gjelstrup, Caroline V. B.; Visser, Andre W.; Stedmon, Colin A.

Published in:
Journal of Geophysical Research: Oceans

Link to article, DOI:
10.1029/2022JC018630

Publication date:
2022

Document Version
Publisher's PDF, also known as Version of record

JGR Oceans

RESEARCH ARTICLE
10.1029/2022JC018630

Separating Annual, Interannual and Regional Change in Sea Surface Temperature in the Northeastern Atlantic and Nordic Seas

Mischa J. M. Saes[1,2], Caroline V. B. Gjelstrup[1], Andre W. Visser[1], and Colin A. Stedmon[1]

[1]National Institute of Aquatic Resources, Technical University of Denmark, Lyngby, Denmark, [2]Now at: Danish Hydraulic Institute, Hørsholm, Denmark

Key Points:

- Seasonal fluctuations in Nordic Seas and Northeastern Atlantic sea surface temperatures explains 90% of the variability
- Both summer maxima and winter minima are warming, with summer temperatures warming twice as fast (0.4 and 0.2°C per decade)
- Other sources of variability include sea-ice melt and switches in large-scale oceanographic conditions in the Northeastern Atlantic

Supporting Information:

Supporting Information may be found in the online version of this article.

Correspondence to:

M. J. M. Saes,
mischasaes@outlook.com

Citation:

Saes, M. J. M., Gjelstrup, C. V. B., Visser, A. W., & Stedmon, C. A. (2022). Separating annual, interannual, and regional change in sea surface temperature in the Northeastern Atlantic and Nordic Seas. *Journal of Geophysical Research: Oceans*, *127*, e2022JC018630. https://doi.org/10.1029/2022JC018630

Received 13 MAR 2022
Accepted 12 AUG 2022

Author Contributions:

Conceptualization: Mischa J. M. Saes, Andre W. Visser, Colin A. Stedmon
Formal analysis: Mischa J. M. Saes, Caroline V. B. Gjelstrup
Funding acquisition: Andre W. Visser, Colin A. Stedmon
Investigation: Mischa J. M. Saes
Methodology: Mischa J. M. Saes, Caroline V. B. Gjelstrup, Colin A. Stedmon
Project Administration: Colin A. Stedmon
Resources: Mischa J. M. Saes
Supervision: Andre W. Visser, Colin A. Stedmon
Validation: Colin A. Stedmon
Visualization: Mischa J. M. Saes
Writing – original draft: Mischa J. M. Saes, Caroline V. B. Gjelstrup

Abstract Sea surface temperature (SST) in the Northeastern North Atlantic and Nordic Seas exhibits pronounced variability across seasonal to decadal time scales. These changes can be expected to be driven by a combination of altered local conditions, shifts in seasonality and large-scale regional oceanographic change. Separating the contribution from each of these offers insight into how the region is changing. Here, we present the result of an analysis of weekly satellite-derived SST data from 1979 to 2020. An empirical orthogonal function (EOF) analysis allows us to separate observed changes in SST into independent underlying timeseries. Each timeseries explains part of the variability in SST. EOF1 can be allocated with changes in seasonality and a long-term warming trend, with summer maxima warming with twice the rate (0.043°C year^{-1}) compared to winter minima (0.023°C year^{-1}). EOF2 is associated with the North Atlantic subpolar gyre and the North Atlantic Oscillation, affecting the Atlantic Water flow across the Greenland-Scotland Ridge, imposing a dipole cooling/warming pattern. Local sea-ice melt along the southeast Greenland shelf is represented by EOF3, and finally the influx of warmer water with the North Icelandic Irminger Current is captured by EOF4. Each of these disaggregated signals differ considerably in their contribution to driving temporal and spatial trends in SST. The isolated signals offer a high-resolution long-time series of valuable indicators of oceanographic change which will likely be reflected in biogeochemistry, plankton, fish, mammals, and seabirds in the region.

Plain Language Summary Sea surface temperature (SST) can be measured by sensors mounted on satellites and this provides a data set with exceptional regional and temporal coverage from 1979 to present. Here, our focus is on examining oceanographic change in the Northeastern Atlantic and Nordic Seas, bordering Greenland, Iceland, and Norway. We apply a data analysis technique that allows us to separate the variability in SST in the region into a series of underlying factors. With this we can resolve: how the seasonal winter minimum temperatures and summer maximum temperatures have been increasing; how conditions in the North Atlantic are driving changes in the region; how increased sea-ice melt is influencing SST; and finally trace the occurrence and impact of an abrupt inflow of warmer water northwards along the west coast of Iceland. Combined these disaggregated factors may help explain changes in the distribution and structure of the marine ecosystem in the region.

1. Introduction

Sea surface temperature (SST) measured by satellites provides a unique time series with high temporal and geographical resolution unparalleled to many other essential ocean variables. Despite its limited penetration depth it can be used as a proxy for the ocean heat content of the mixed layer (Chen & Tung, 2018). As a result, variations in SST can be linked to changing positions of oceanographic fronts (Raj et al., 2019; Sutherland & Pickart, 2008), variability in upwelling (Lentz & Largier, 2006) or deep convection (de Jong & de Steur, 2016) and warming of surface waters as a result of climate change (Masson-Delmotte et al., 2019). Variations in SST can also indicate initiation of larger changes in regional marine ecosystems as oceanographic change can have a cascading impact on all trophic levels in ecosystems (Hátún et al., 2009).

The Northeastern Atlantic and Nordic Seas are characterized by distinctive domains in the average SST and its variability (Figures 1 and 2). The shelf waters in the west are influenced by Polar Waters brought south from the Arctic Ocean with the East Greenland Current (EGC). SST is cold either due to its Arctic origin, or contribution from seasonal ice melt from both sea-ice and the Greenland ice sheet. Part of the southward flowing surface EGC deviates eastward, where it affects the surface waters in the Nordic Seas (Jeansson et al., 2017). Once past the

Writing – review & editing: Caroline V. B. Gjelstrup, Andre W. Visser, Colin A. Stedmon

Denmark Strait, the EGC is confined to the shallow, narrow region along the southeast Greenland coast. Further inshore, a low salinity southward flowing surface jet known as the East Greenland Coastal Current (EGCC) resides (Bacon et al., 2014; Sutherland & Pickart, 2008).

In the eastern part of the region surface waters are dominated by the comparatively warm and saline Atlantic Water (AW) flowing poleward with the North Atlantic Current (NAC). Part of this current continues northwards into the Norwegian Sea as the Norwegian Atlantic Current (NwAC) inducing a strong SST gradient across the Nordic Seas (Figure 1) (Orvik & Niiler, 2002). Some of the NwAC diverges into the Barents Sea, while the remainder continues north entering the Arctic Ocean via the West Spitsbergen Current (WSC) in the Fram Strait (Orvik & Niiler, 2002). Here, about half of the flow recirculates turning west and merging with the EGC to continue southwards as Return Atlantic Water (Bourke et al., 1988; Hattermann et al., 2016; Jeansson et al., 2017; Raj et al., 2019).

The region south of the Greenland-Scotland Ridge (GSR) is dominated by the cyclonic Subpolar Gyre (SPG). The NAC comprises the southern and eastern boundary currents of the gyre. As the NAC enters the Subpolar North Atlantic (SPNA) it separates into branches; one flows over the Rockall Plateau and the Rockall Trough between Iceland and Ireland, one enters the Iceland Basin and one recirculates southward to eventually re-join the subtropical gyre (STG) (Daniault et al., 2016). The Irminger Current (IC) separates from the northward flow in the Iceland Basin and turns westward toward east Greenland. South of the Denmark Strait, the IC bifurcates with a smaller portion flowing northwards through Denmark Strait and along the western and northern coast of Iceland as the North Icelandic Irminger Current (NIIC). The larger part turns south and flows along the east Greenland shelf break parallel to the EGC. Sharp oceanic fronts develop between the IC, EGC, and EGCC (Hátún et al., 2005). A portion of this flow will remain in the Irminger Sea, as it recirculates near Cape Farewell, while another portion will round Cape Farewell to continue north along western Greenland.

In addition to advection of ocean currents, SST in the Northeastern Atlantic and Nordic Seas is strongly influenced by heat exchange with the atmosphere, sea-ice and associated melt water, and upward heat fluxes from deeper warm waters (Carvalho & Wang, 2020; Furevik, 2000). Based on the HadISST data set, Meredith et al. (2019) show a warming trend in the Northeastern Atlantic and Nordic Seas over the 1982–2017 period. Barton et al., 2018 and Asbjørnsen et al. (2020) also show recent SST increase in the northern Nordic Seas and Barents Sea. In contrast, the Irminger Sea experienced a decline in SST between 2007 and 2016 (Broomé et al., 2020; Figure 2), indicating a disconnect between the Northeastern Atlantic and Nordic Seas over this period. A linear regression analysis of SST over the 2007–2020 period clearly reflects these patterns in the region (Figure 2). In the Greenland Sea, the warming trend can be up to 0.15°C per year and appears to be persistent across the year. South of Iceland, significant cooling over the SPG is apparent. The observed cooling is largest in summer, with rates toward −0.15°C per year (Figure 2). Regions where no significant linear relationship is found (yellow patterns in Figure 2) clearly reveal the frontal zones between water masses (Orvik & Niiler, 2002), in particular boundaries of the EGC and EGCC toward the west and the propagation northwards and subsequent dissipation of a front in the southeast of the region during the transition from winter to summer (Figure 2).

Several mechanisms have been invoked to explain the observed trends in regional water temperatures. These include large-scale atmospheric forcing such as the North Atlantic Oscillation (NAO), fluctuations in the SPG circulation, changing wind speeds, and variable sea-ice concentration (Broomé et al., 2020; Carvalho & Wang, 2020; Furevik, 2000). The aim of this study is to carry out a holistic analysis of SST of the region by applying an Empirical Orthogonal Function (EOF) analysis also known as a principle component analysis. SST is hypothesized to be responding to a combination of altered local conditions, potential shifts in seasonality and large-scale regional oceanographic change, which will materialize as a linear combination of factors influencing surface water heat content. The analysis allows us to isolate the contribution of underlying independent (orthogonal) factors to the observed SST changes with no assumption on temporal or regional trends. Separating the contribution from each of these offers insight into how the region is changing and also offers factors which we propose can be linked to additional shifts in distribution and diversity of marine organisms, from phytoplankton up to marine mammals.

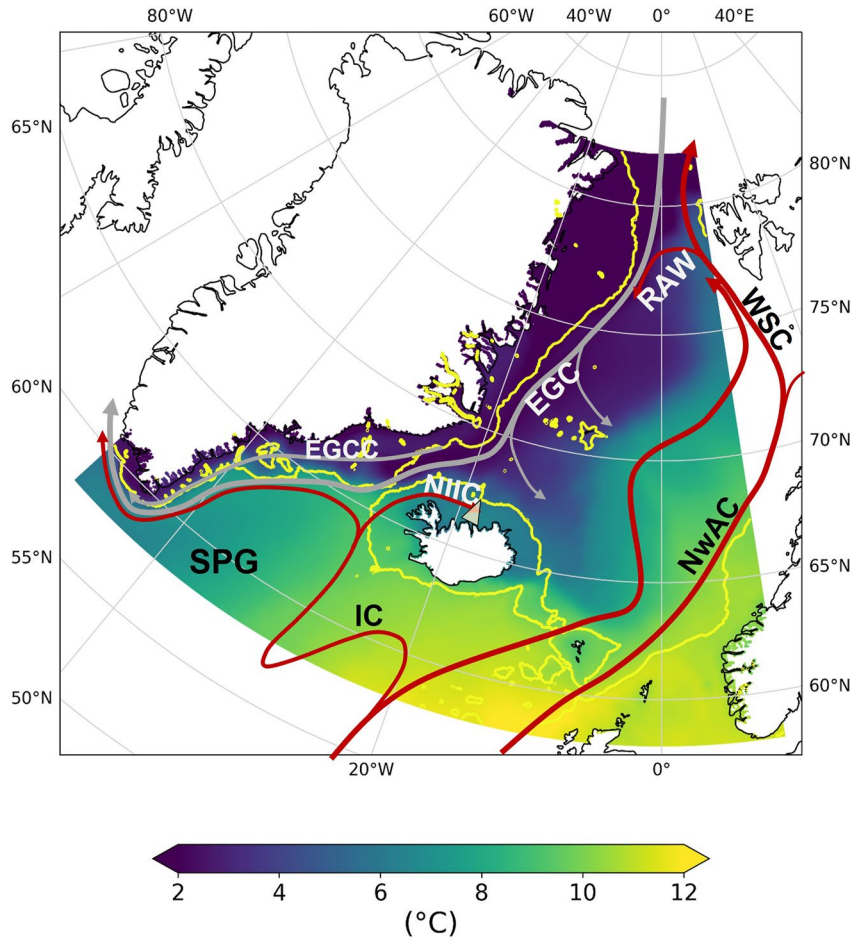

Figure 1. Average sea surface temperature calculated from 2007 to 2020 daily values derived from "Operational Sea Surface Temperature and Sea Ice Analysis (OSTIA)," developed by the Met Office (Table 1). Yellow contours indicate the 500 m isobath and red and gray arrows indicate major warm and cold surface circulation features in the region, respectively. The position of the Siglunes transect is denoted by the triangle on the north Iceland shelf.

2. Materials and Methods

The region of interest expands between 48°W and 9°E, and 58° to 82°N. Two Copernicus SST data sets with coverage of the region were used in the analysis (Table 1). The first was a near-real time data product derived across different satellite platforms called "Operational Sea Surface Temperature and Sea Ice Analysis (OSTIA)," developed by the Met Office. The product is identified as "SST_GLO_SST_L4_NRT_OBSERVATIONS_010_001" (Donlon et al., 2012; Good et al., 2020; Stark et al., 2007). It uses satellite data provided by the GHRSST framework (Group for High Resolution SST) and has global coverage on a 0.05° (approximately 6 km along the north-south axis in region of interest, and between 800 m and 3 km in the east-west direction) resolution grid and includes daily sea surface foundation temperature data (temperature of upper 10 m of the ocean, free of diurnal temperature variations), sea-ice cover and analysis error for the 2007–2020 period. In order to remove bias errors, the satellite observed SST has been compared with in-situ SST measurements (drifting buoys) and ENVISAT Advanced Along Track Scanning Radiometer (AATSR) SST observations (Donlon et al., 2012). As a result, an uncertainty value (in Kelvin), is provided for each location at every time step. The high spatial resolution allows one to identify fine structures in the position of fronts (Figure 2).

To extend the temporal coverage to 1979, the ERA5 reanalysis data set provided by the European Center for Medium-Range Weather Forecasts (ECMWF) and available via Copernicus Climate Change Service data portal was used (Hersbach et al., 2018). This data set is derived from a combination of observational and model data to

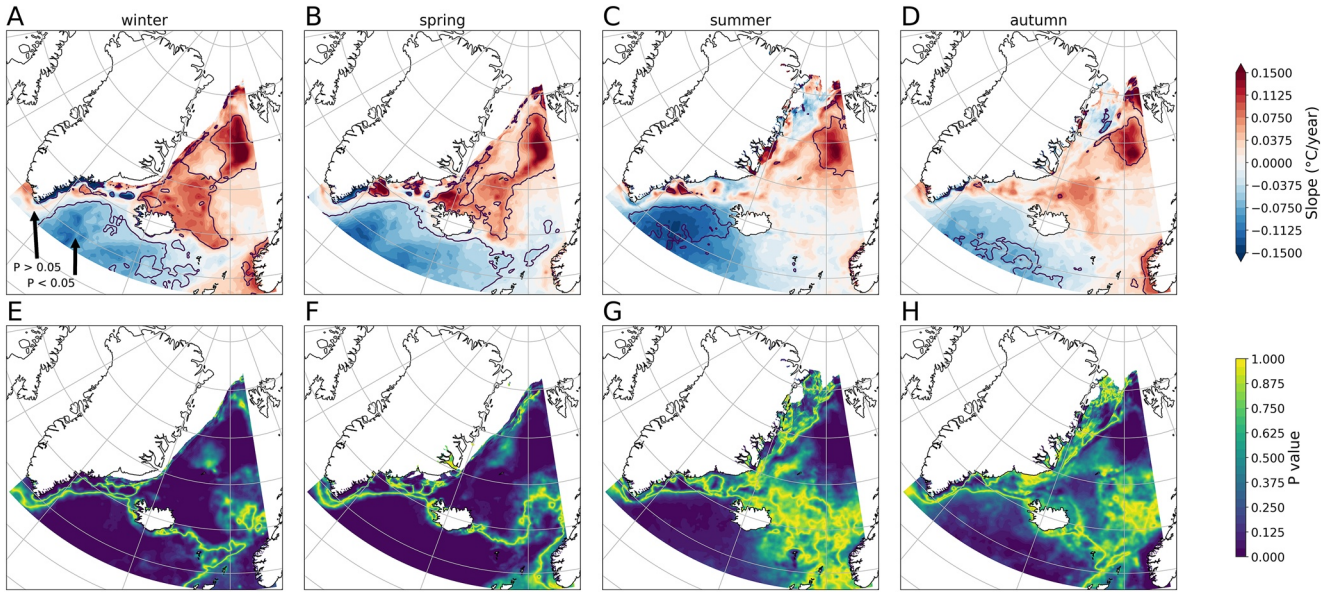

Figure 2. Results of a linear regression across the OSTIA data set from 2007 to 2020 segregated by season: Winter (December to February); spring (March to May); summer (June to August) and autumn (September to November). Top row shows the slope of the regression. Isolines indicate the division between significant ($p < 0.05$) and nonsignificant regression slopes. The bottom row presents maps of the p-value for the regressions.

form a complete spatial and temporal series provided at 0.25° (approximately 27 km in the region of interest along the north-south axis, and between 4 and 15 km) horizontal and hourly temporal resolution (Dee et al., 2014).

2.1. Data Preprocessing and EOF Analysis

In contrast to the linear regression analysis (Figure 2), EOF analyses cannot be applied to data sets with missing data points. While interpolation with bordering (temporal and spatial) measurements can produce visually acceptable results, they do not actually aid the EOF analysis by providing additional information. In fact, this can potentially impair the separation of underlying features as signal noise and variability is averaged and combined. Missing data in the near real time (NT) data set stems for the most part from the presence of sea-ice. Before EOF analysis, all data points with a sea-ice fraction greater than 25% were discarded. These corresponded to data points already flagged with a high measurement error. An ice mask was then generated which excluded data from areas where there has been ice coverage. Due to the inclusion of models, the ERA5 data set extrapolates below the sea-ice, offering the potential to include ice covered waters, thereby introducing a discrepancy in EOF results from the two data sets. The application of an identical ice mask to both data sets resulted in comparable EOFs (Figures S1–S4 in Supporting Information S1). As the ERA5 data set has superior temporal coverage the EOF analysis presented from here onwards is based on the ERA5 reanalysis. The data was down-sampled to weekly averages and organized into a matrix with geographical location as columns and temporal series as rows. Before performing the EOF analysis the data was centered (mean subtraction) and scaled (normalized to SD) by location to ensure equal weighting of data from different regions.

Table 1
SST Datasets and Their Key Characteristics Used in This Study

Data set type	Parameter	Coverage	Temporal resolution	Timespan in study	Spatial resolution
OSTIA near-real time	Foundation SST	Global	Daily	2007–2020	0.05°
	Sea-ice fraction	Global	Daily	2007–2020	0.05°
	Analysis error	Global	Daily	2007–2020	0.05°
ERA5 Reanalysis	Foundation SST	Global	Hourly	1979–2020	0.25°
	Sea-ice fraction	Global	Hourly	1979–2020	0.25°

With the EOF analysis, we separate SST variability in space and time into a number of orthogonal components each having a geographical loading and a temporal score. The product of the loadings map, score time series for a given component, and the SD map of the original data allows us to back-calculate the temperature variation represented by the component (i.e., the given components contribution to temperature anomaly).

2.2. Climate Variables

To assess the potential driving forces of the temporal development in the EOFs, several climate indices were gathered. A SPG index based on multiple linear regression of the first and second modes of North Atlantic sea surface height variability was used as an indicator of the strength and shape of the subpolar gyre. The index was derived by Chafik (2019) and gathered from the Bolin Center for Climate research: https://bolin.su.se/data/chafik-2019-3. The North Atlantic Oscillation (NAO) index is based on the atmospheric pressure difference between Iceland and the Azores and conditions in the study region can potentially be correlated to this as it influences North Atlantic temperature and precipitation patterns (Barnston & Livezey, 1987; W. Y. Chen & van den Dool, 2003; Hurrell, 1995; van den Dool et al., 2000). A monthly time series of the NAO index was obtained from NOAA.

3. Results

Almost 95% of the observed variation in SST is explained by the first four components from the EOF analysis (Figure 3). Systematic patterns in their geographic distribution and temporal signal indicate that they are linked to specific phenomena and offer confidence in the robustness of the result. The robustness of the derived EOF components was further confirmed by re-running the EOF decomposition on de-seasoned SST, which resulted in comparable components (Figure S5 in Supporting Information S1). The largest portion (90%) of the variability in the region can be attributed to seasonal warming and cooling. The EOF1 loading map is largely featureless (Figure 3a) indicating that this component is of equal importance for the entire study area and likely driven by atmospheric forcing. The one exception is a narrow band along the edge of the sea-ice mask, where the loading is slightly lower. A reconstruction of SST anomalies imposed by this component (Figure 3b) shows a strong imprint of seasonality with variability around the mean of more than 6°C. In order to assess if there has been a change in the timing and intensity of seasonal maxima and minima, the temperature anomaly for EOF1 was plotted by year and week (Figure 4a). A regression analysis indicates that there has been no significant change in timing across the years (p-value > 0.05), as would be expected. Also apparent is a positive linear trend in both the summer maximum (0.043°C year^{-1}) and winter minimum (0.024°C year^{-1}) SST (Figure 4b). Note, that the rates provided on Figure 4 were calculated specifically for the Irminger Sea location, but are very similar across the entire region as the EOF1 loadings are evenly distributed (Figure 3a). These results show that SST increased with twice the rate in summers compared to winters over the course of 41 years.

The time series associated with EOF1 is also characterized by a shift toward higher temperatures in 2000 that persists through to the end of the time series (Figure 4c). A Chow test was done to gauge whether the EOF1 time series is best described with a single linear regression model through the entire time series (Figure 4b), or if the description of the time series significantly improves when using two regression models, one on either side of the identified shift. The Chow test concludes that the time series representation is significantly better when sectioned into two around August 2000 (Figure 4c) (p-value < 0.01), thus confirming the existence and timing of the identified shift.

The second EOF explains approximately 2.6% of the observed variation in SST and is opposite in sign pivoting north-south approximately at the latitude of Iceland. This spatial pattern has a high degree of similarity to the linear trends presented in Figure 2. This gives confidence that the dipole nature of EOF2 is a real feature of SST variability in the Northeast Atlantic rather than an artifact introduced by the constraints of the EOF approach itself. The reconstructed SST anomalies from EOF2 show a contribution to SST variability of more than 2°C. The time series is characterized by three periods: (a) a period from 1979 to 1995 where there are variable anomalies; (b) a period from 1995 to 2014 where temperature anomalies in the north are and remain persistently colder, and conversely persistently warmer in the south; and (c) a period from 2014 to 2020 where anomalies changed to be persistently warmer and cooler in the north and south respectively. These fluctuations hint at a possible linkage to regional climate indices such as the SPG and NAO indices. A correlation analysis found relations between EOF2 scores and both the NAO (-0.41, p-value < 0.01) and the SPG (-0.67, p-value < 0.01) indices at 5 and 4 weeks

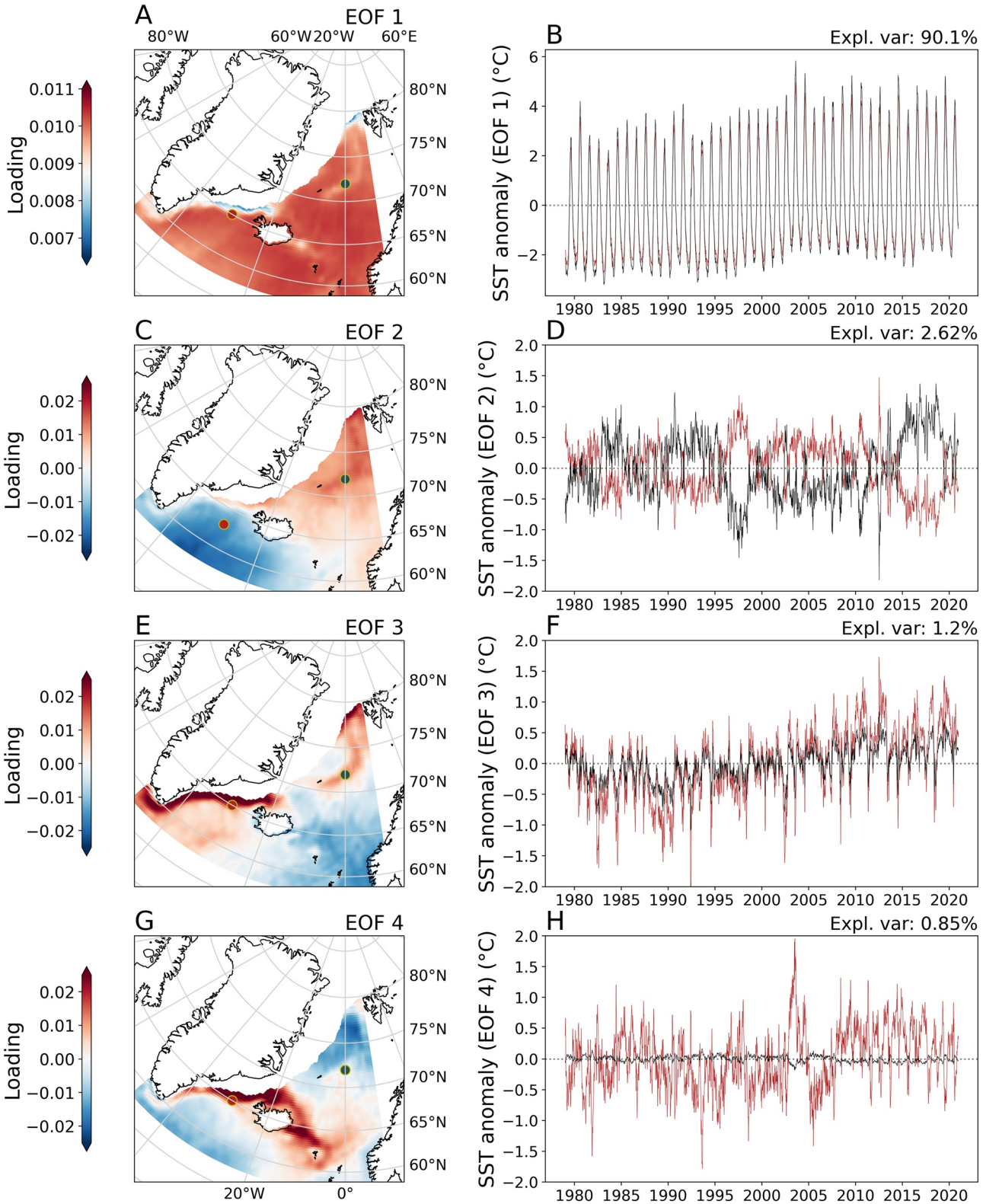

Figure 3. First four Empirical Orthogonal Functions derived from the analysis of the ERA5 SST data set. The maps to the left indicate the geographical loadings and the plots on the right represent the contribution of each component to the SST anomaly for selected locations (red and black). The locations for the plotted SST anomalies are shown on each of the maps (red and black dot).

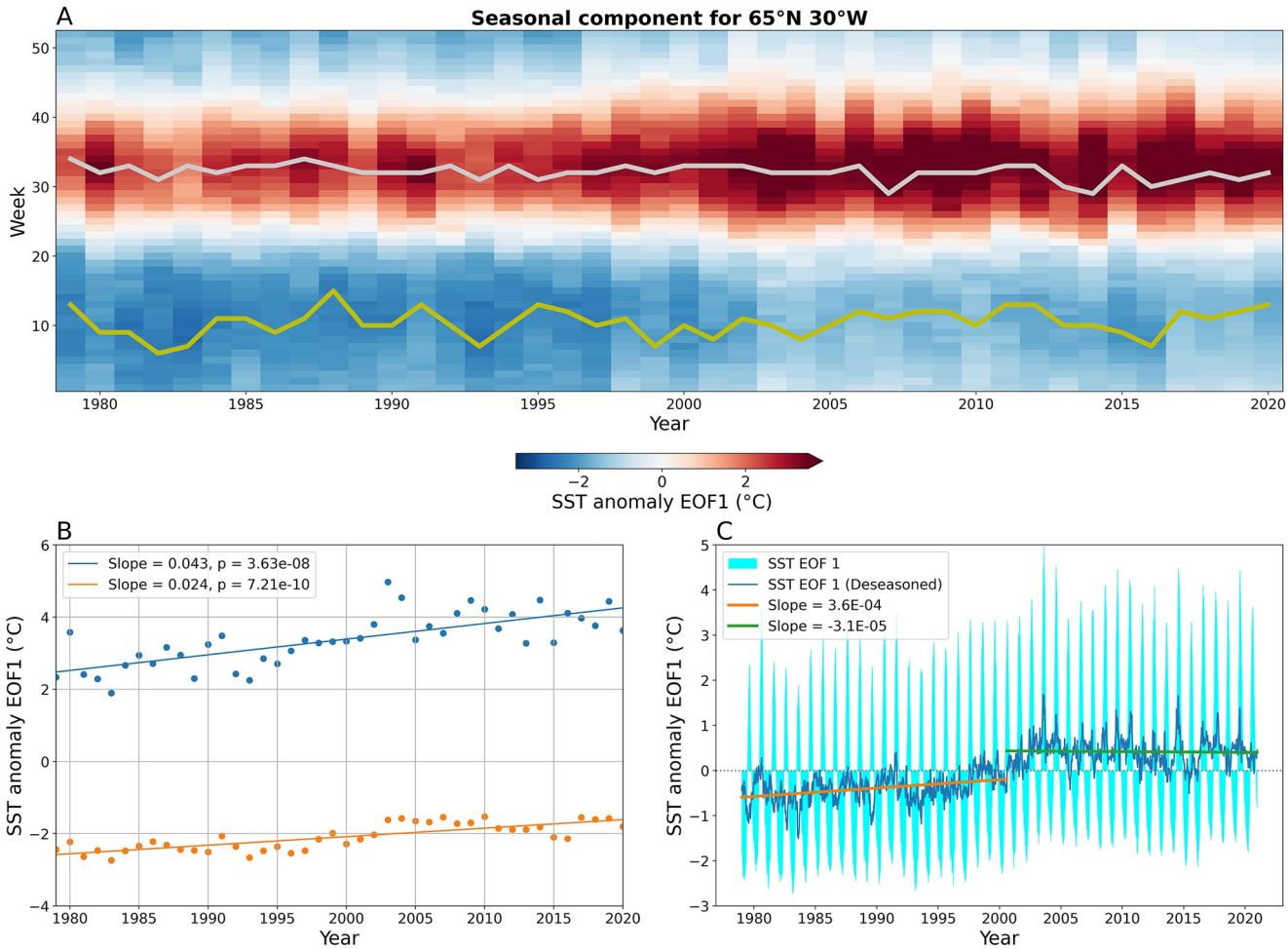

Figure 4. Analysis of temporal developments in the seasonality represented by EOF1. (a) Hovmöller plot of the development of temperature anomaly assigned to EOF1 across the year and over the time series. Gray and yellow lines represent the timing of the summer maximum and winter minimum, respectively. (b) Development of the annual summer maxima and winter minima across the time series. (c) Analysis of de-seasoned scores revealing two distinct periods. Linear regression lines are presented for the period 1979–2000 (orange line) and the period 2000–2020 (green line).

lag, respectively (Figure 5). Lag times with the highest correlation were determined from cross-correlation analysis. It is clear that the segregations of the time series of EOF2 into three periods agrees with trends in the two indices (Figure 5). In particular the middle period spanning from 1995 to 2014 where the NAO and SPG indices are persistently negative, and the final period where there is a systematic change to positive values (note both indices are plotted with inverted axes in Figures 5b and 5d).

Variability in SST within a narrow band spanning the length of the southeast Greenland shelf was captured by EOF3, which contributes 1.2% of the total variation in SST (Figure 3e). This band broadly corresponds to the area with low seasonality (EOF1, Figure 3a), indicating that it has a more unique variability not directly related to the large-scale seasonal warming and cooling explained by EOF1. Figure 3f indicates that these waters have experienced a systematic long-term warming across much of the time series, in particular from the late 1980s (approximately 1°C increase over a 40 year period). Furthermore, reconstructed SST also indicates high-frequency variability linked to seasonal trends (Figure 6). The SST anomaly explained by EOF3 is lowest in summer months within the band of high loadings along the edge of the sea-ice mask (Figure 6). An analysis of the timing of the summer minimum (similar to that done for EOF1) indicated that there has been no significant systematic shift over the time period. As can be seen in Figure 6, the timing of the minimum is variable and ranges between late May and late June. Both the seasonal maxima and minima experience a comparable SST increase (e.g., 0.025 and 0.022°C year^{-1}, respectively at 65°N and 30°W) through the entire 41 year study period, indicating that the

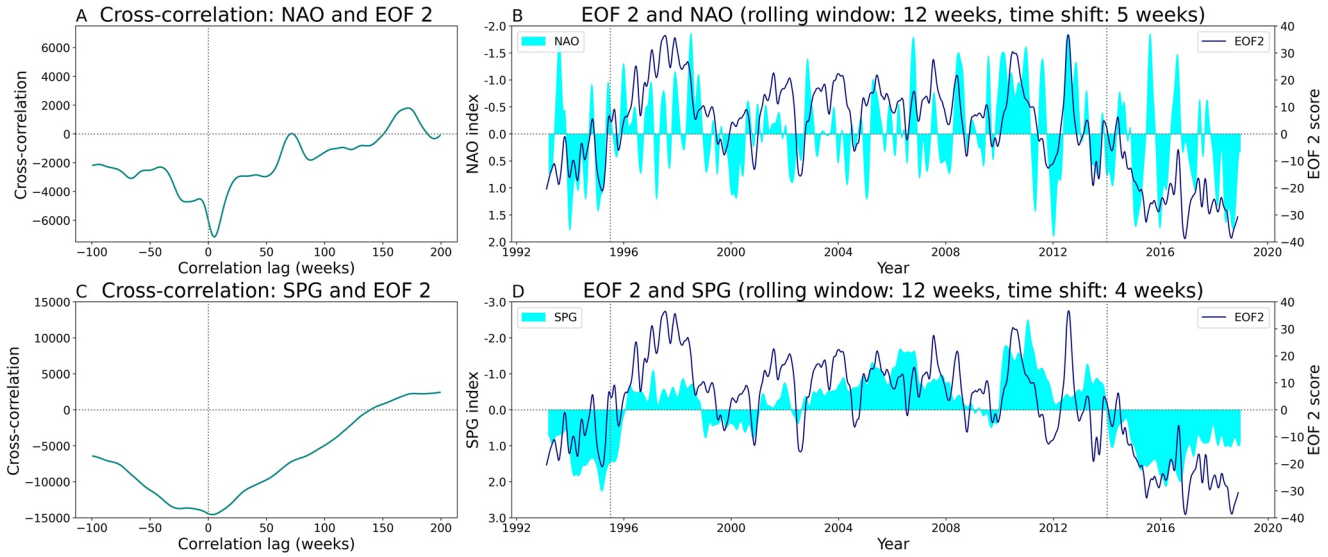

Figure 5. Comparison of the time series of EOF2 with NAO and SPG. Cross-correlation analysis of EOF2 with NAO (a) and SPG (c) revealed a 4 and 5-week lag, respectively. Panels (b) and (d) compare EOF2 and the two indices. A 12 week rolling average with a cosine window is applied on both the EOF2 and the NAO and SPG time series. Both NAO and SPG were recalculated from monthly to weekly time series. The vertical lines in panels (b) and (d) (1995 and 2014) mark transition in the NAO and SPG indices.

long-term trend is the same for both summer and winter. The intensity of this long-term trend, however, varies spatially as reflected in the EOF3 loading (Figure 3f).

The fourth EOF is largely confined to the region along the Greenland-Faroe Islands ridge with greatest values northwest and southeast of Iceland (Figure 3g). Figure 3h shows the time series of the SST anomaly explained by EOF4 for two selected points, one near Denmark Strait and another in the Greenland Sea. From this, it is clear that EOF4 is focused on the changes occurring in Icelandic waters (red line in Figure 3h). The time series is characterized by two frequencies: a high frequency variability which was found not to be linked to seasonality; and a lower frequency change. The latter appeared to represent somewhat stable conditions before 2003, a positive excursion

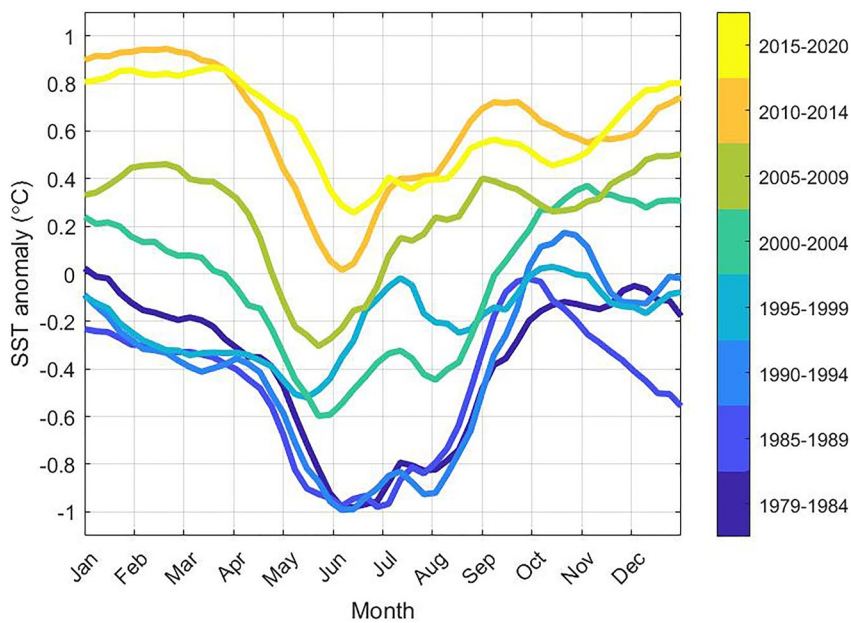

Figure 6. Weekly mean seasonal SST anomalies explained by EOF3 in the Irminger Sea (31°W, 65°N, Figure 3e red dot) averaged over 5 years intervals.

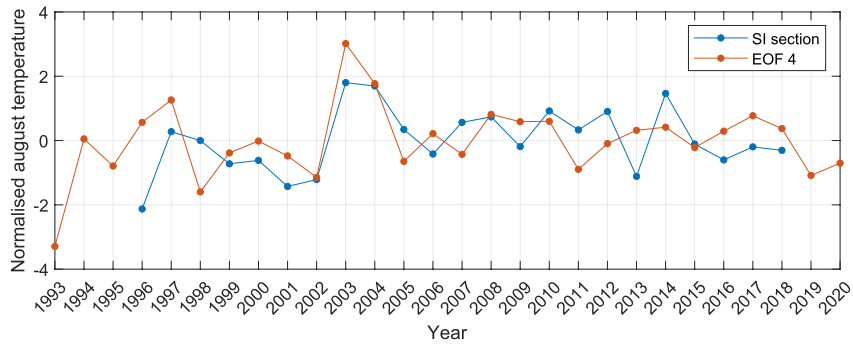

Figure 7. Normalized mean August temperature at the Siglunes transect (blue) and SST anomalies induced by EOF4 at the same location (red). Data from the Siglunes transect at approx. 67.75°N, 18.83°W (triangle on Figure 1) collected by the Marine and Freshwater Research Institute were downloaded from SeaDataNet (https://cdi.seadatanet.org/search).

in SST up to 2°C between 2003 and 2005 followed by a brief return, then a persistently positive SST anomaly from 2007 onwards (Figure 3h). The 2007 shift is confirmed by a change point detection procedure similar to that done for EOF1. Comparison of this time series with measurements from the Icelandic monitoring program indicates that the warm SST anomaly in 2003 and 2004 captured in EOF4 corresponds well with observations as supported by a relatively high correlation coefficient ($R^2 = 0.47$, p-value = 0.02; Figure 7).

4. Discussion

The decomposition of SST into its linear components has partitioned SST changes into that due to altered seasonality captured in EOF1 and EOF3 and that linked to variable oceanic advection captured in EOF2 and EOF4.

4.1. Seasonal Control of SST

The seasonal warming and cooling of the ocean surface is the major determinant of SST variability in the SPNA and Nordic Seas. Although the timing of the seasonal maximum and minimum has not changed over the 40-year period considered here, the intensity of seasonal warming and cooling has (Figure 3). Annually the region is a net source of heat to the atmosphere (Serreze et al., 2007). Cooling of surface waters from September to March exceeds the warming that occurs from April to August (Serreze et al., 2007). EOF1 indicates that winter SST has been rising at a rate of 0.024°C per year and summer SST at a rate approximately twice that throughout the region. These warming rates are in good agreement with those reported for March (0.2°C per decade) and September (0.4°C per decade) over the period 1982–2017 in Meredith et al. (2019). The findings reveal two changes that are occurring in the seasonal component of SST in the region. The fact that summer and winter temperatures are increasing suggests that there is a general increase in heat transport into the region. However, this does not explain why summer maxima are warming faster than winter minima. This could in turn be reflecting a decrease in the summer mixed layer depth. As SST increases the mixed layer depth can be expected to shoal, assuming that the warming of surface water dominates the density change, rather than change at depth (Somavilla et al., 2017).

Strong seasonal variability is also evident in the annual build-up and melt of sea-ice. Summertime sea-ice melt along the east Greenland shelf absorbs considerable amounts of latent heat, and releases cold, fresh waters initially lowering summer SST in the western part of the Nordic Seas (Smedsrud et al., 2022). This is reflected in the high frequency signal captured in EOF3 (Figure 6). This component thereby serves as a local, geographical correction to the seasonal pattern identified by EOF1. Since EOF3 mainly serves as a summertime correction, it should not be seen as an absolute summer cooling. It merely modifies the seasonal trend in EOF1 to represent a local delay/reduction of the summer heating along the ice front, possibly due to sea-ice meltwater or polar waters transported in the EGC. The general increase in SST along east Greenland observed in EOF3 (apparent as a baseline shift in Figure 6) is comparable to that seen for winter SST in EOF1. The similarity of the interannual trends embedded in EOF1 and EOF3 suggests that these components have a common driver.

4.2. Regional Connectivity

Although seasonal heating and cooling of the surface drives the majority of SST variability, advection of warm, saline AW into the Nordic Seas is responsible for imposing important regional differences. Since EOF1 represents seasonal variability, it is reasonable to assume EOFs 2 and 4 to be related to oceanic advection and interannual variability, which will be considered in the following. AW exchange between the SPNA and Nordic Seas is facilitated via three main inflow pathways: (a) flow through the Faroe-Shetland Channel, (b) flow between Iceland and the Faroe Islands, and (c) inflow with NIIC through Denmark Strait (Hansen & Østerhus, 2000; Østerhus et al., 2019). All three inflow pathways contribute to the substantial increase (21 TW) in ocean heat transport in 1998–2002 identified in Tsubouchi et al. (2021). The authors furthermore characterize this abrupt increase as a change-point similar to that reported for EOF1 in the current study (Figure 4c and Figure S2 in Supporting Information S1) suggesting that the identified 2000 shift in EOF1 represents increased oceanic heat transport across the GSR. As part of the variability in the inflow of warm waters is set upstream in the NAC, one can expect variability in the three inflows to be correlated and resolved as a single EOF. This is for the most part true, as seen for EOF2, however, the isolation of an additional contribution, more specific to the NIIC (EOF4), reveals a local component which is not directly correlated.

Although AW transport with the NIIC is the smallest of the three through-flows, it is the primary source of heat and nutrients to the north Iceland shelf (Figure 1; Hansen & Østerhus, 2000). High variability due to translation of fronts is inherent to this area (Figures 2e–2h), and fluctuations in the temperature and volume of the AW inflow with the NIIC have been used to explain variable temperature and heat transport to the shelf (Casanova-Masjoan et al., 2020; Jónsson & Valdimarsson, 2012; Zhao et al., 2018). Based on mooring observations Jónsson and Valdimarsson (2012) captured an anomalously strong NIIC inflow event between 2003 and 2004, which concurs with the temperature excursion in the fourth component derived here (Figure 7). Previous studies concerning the NIIC furthermore document a shift to persistently elevated temperatures after 2007 compared to conditions before the 2003 warm event (Casanova-Masjoan et al., 2020; Zhao et al., 2018). A similar shift was noted in EOF4 (Figure 7), which supports our interpretation of EOF4 as representative of AW inflow with the NIIC.

East of Iceland, the NwAC carries heat and salt across the Iceland-Scotland ridge and into the Norwegian Sea. Consistent with numerous previous studies relating interannual variability in inflow properties and volume to large-scale wind forcing patterns (e.g., Bringedal et al., 2018; Sandø et al., 2012), we found a significant correlation (-0.41, p-value < 0.01) between NAO and EOF2 (Figure 5d). Strengthened westerlies under positive NAO cause elevated heat loss and negative SST anomalies over the SPNA (Sarafanov, 2009; Visbeck et al., 2003). Simultaneously, the intensified atmospheric circulation transports more warm, moist air northwards and increases AW inflow with the NwAC, invoking positive SST anomalies in the eastern Nordic Seas (Dickson et al., 2000; Furevik, 2000; Mikhailova et al., 2021). As demonstrated by Deser et al. (2010), a dipole SST pattern between the SPNA and Nordic Seas consequently develops under positive NAO forcing. Whilst the correlation between NAO and EOF2 is significant, the robustness of this relationship is questionable as the strength of correlation is highly sensitive to the length of the smoothing window.

Other studies have attributed variable inflow properties to changes in the strength and shape of the SPG (e.g., Hátún et al., 2005; Kenigson & Timmermans, 2021; Lozier & Stewart, 2008). A strong correlation (-0.67, p-value < 0.01) with the SPG index suggests that SPG dynamics are indeed manifested in the development of regional SST patterns (Figure 5). Shifts in the position of the subarctic front, commonly referred to as expansion/contraction of the SPG have been invoked to explain decadal temperature trends in the SPNA and variable composition of inflow across the GSR (Desbruyères et al., 2021; Hátún et al., 2005; Kenigson & Timmermans, 2021). Weak SPG circulation is associated with contraction of the SPG and expansion of the STG, effectively displacing the subarctic front northwestwards, and allowing for a wider passage for warm, saline subtropical waters to penetrate the eastern SPNA and flow into the Nordic Seas (Häkkinen et al., 2011). Conversely, during strong SPG circulation, subtropical waters are blocked by the now expanded SPG, rerouting the subtropical waters southwards (Häkkinen & Rhines, 2004). The Atlantic inflow to the Nordic Seas is in this case comprised of an increased ratio of cold, fresh SPNA source waters compared to STG waters. Accordingly, the SPG index and SST anomalies in the SPNA are inversely correlated in agreement with Hátún et al. (2005).

However, whilst the SPNA has been cooling since the mid 2000's in accordance with the expanded state of the SPG, the Nordic Seas have not (Figures 2 and 5). A possible explanation for this apparent disconnect is that

the SPNA cooling had simply not reached the Nordic Seas by 2014. According to Holliday et al. (2008) NAC anomalies are detectable in the southern Norwegian Sea approximately 1 year after crossing the Faroe-Shetland Channel, and appear south of Svalbard 3 years later. In another study, Kenigson and Timmermans (2021) suggest a lag of 5 years between the development of freshwater content anomalies in the SPNA and a measurable change in the Nordic Seas. It is therefore possible that the dipole fingerprint associated with EOF2 is the consequence of slow propagation and mixing time scales of temperature anomalies generated by changing states of the SPG. Broomé et al. (2020) offer an alternative explanation for the SPNA-Nordic Seas disconnect. The authors suggest that the connection between the SPNA and Nordic Seas is time varying as they show that correlation between temperature in the eastern Nordic Seas and SPNA is only significant along the subtropical AW pathway. Thus, the SPNA-Nordic Seas connection is strong under contracted gyre conditions but not when the SPG is expanded. This notion highlights that SPNA and Nordic Seas exchanges across the GSR are not yet fully understood (Bringedal et al., 2018).

In contrast to the derived EOFs, the physical processes driving observed changes are not necessarily independent (orthogonal) of each other. Therefore, it is possible that both NAO and SPG associated changes are manifested in EOF2. While we have only speculated the mechanism causing the dipole spatial pattern associated with EOF2, it is clear that AW inflow patterns are important drivers of SST variability in the SPNA and Nordic Seas.

The increased ocean heat transport as represented by the shift in EOF1 in 2000 and the de-seasoned EOF model (Figure S2 in Supporting Information S1), the "switching" role of the SPG and increased AW inflow with the NIIC, collectively suggest an increase in the oceanic heat transport to the Nordic Seas over the 1979–2020 period. These findings are aligned with a suite of recent studies on the heat budget of the Nordic Seas recently reviewed by Smedsrud et al. (2022) and provide a separation of the response in SST into independent underlying factors. Increases in AW inflow in part contradict evidence for decreases in Atlantic meridional overturning circulation (AMOC) (e.g., Smeed et al., 2018), which are based on deepwater moorings further south. This apparent disconnect between observations from the subtropics and Nordic Seas is also noted in Tsubouchi et al. (2021) and highlights the fact that linkages between the subtropics and higher latitudes are yet to be resolved.

5. Conclusions

Sea surface conditions are the result of the complex interplay between atmosphere and ocean. SST's are subjected to large-scale atmospheric patterns (e.g., NAO), short-term cycles (e.g., day/night cycles), intermediate-term cycles (e.g., seasonal) cycles, and long-term cycles (e.g., strengthening and weakening of the AMOC). Our results show that EOF analysis is a robust method for disentangling both spatial and temporal patterns in SST, enabling us to attribute change to specific processes acting on various timescales and differing in geographic extents. This has implications for the predictability of SST conditions and their impacts in the Northeastern Atlantic and Nordic Seas. From the EOF analysis, we isolate a dominant seasonal signal revealing that summer maximum SST is increasing at about twice the rate of winter minima warming (EOF1), potentially reflecting a shallowing of the summer mixed layer depth. Furthermore, the impact of NAO and the SPG on regional SST is isolated (EOF2). This is of major importance as it impacts the intrusion of warm AW into the Nordic Seas with consequence for climate and ecosystems in the region. More local effects on SST, such as the impact of sea-ice melt along the ice edge were also captured in the analysis (EOF3). Finally, EOF4 relates to variable AW heat transport onto the north Iceland shelf with the NIIC.

The influence of each of these independent SST components on regional SST trends varies considerably throughout the region and across the time period considered. Individually, the EOF components pose as high-resolution time series of oceanographic change that is likely also reflected in biogeochemistry, plankton, fish, mammals, and seabirds in the region. We therefore suggest that some of EOF components presented here may provide useful proxies: EOF3 may be regarded as an indirect indicator of the impact of sea-ice melt, whereas EOF4 represents a proxy for influx of warm nutrient-rich AW to the north Iceland shelf.

Data Availability Statement

The OSTIA and ERA5 data sets used in this paper are available from at: https://doi.org/10.48670/moi-00165 and https://doi.org/10.24381/cds.adbb2d47, respectively. CTD data from the Siglunes section and the first four EOF components derived are freely available at data.dtu.dk via https://doi.org/10.11583/DTU.19316264.

Acknowledgments
Colin A. Stedmon acknowledges received funding from the Independent Research Fund Denmark Grant Nos. 9040-00266B and the Nordic Council of Ministers AG-Fisk Grant number (209)-2020-LEGCO. Andre W. Visser acknowledges funding from Horizon2020 Project ECOTIP (Grant agreement #869383).

References

Asbjørnsen, H., Årthun, M., Skagseth, Ø., & Eldevik, T. (2020). Mechanisms underlying recent Arctic Atlantification. *Geophysical Research Letters*, *47*(15). e2020GL088036. https://doi.org/10.1029/2020GL088036

Bacon, S., Marshall, A., Holliday, N. P., Aksenov, Y., & Dye, S. R. (2014). Seasonal variability of the East Greenland coastal current. *Journal of Geophysical Research: Oceans*, *119*(6), 3967–3987. https://doi.org/10.1002/2013JC009279

Barnston, A. G., & Livezey, R. E. (1987). Classification, seasonality and persistence of low-frequency atmospheric circulation patterns. *Monthly Weather Review*, *115*(6), 1083–1126. https://doi.org/10.1175/1520-0493(1987)115<1083:csapol>2.0.co;2

Barton, B. I., Lenn, Y. D., & Lique, C. (2018). Observed Atlantification of the Barents Sea causes the polar front to limit the expansion of winter sea ice. *Journal of Physical Oceanography*, *48*(8), 1849–1866. https://doi.org/10.1175/JPO-D-18-0003.1

Bourke, R. H., Weigel, A. M., & Paquette, R. G. (1988). The westward turning branch of the west Spitsbergen current. *Journal of Geophysical Research*, *93*, 14065. https://doi.org/10.1029/JC093iC11p14065

Bringedal, C., Eldevik, T., Skagseth, Ø., Spall, M. A., & Østerhus, S. (2018). Structure and forcing of observed exchanges across the Greenland-Scotland ridge. *Journal of Climate*, *31*(24), 9881–9901. https://doi.org/10.1175/jcli-d-17-0889.1. Retrieved from https://www.jstor.org/stable/26661469

Broomé, S., Chafik, L., & Nilsson, J. (2020). Mechanisms of decadal changes in sea surface height and heat content in the eastern Nordic Seas. *Ocean Science*, *16*(3), 715–728. https://doi.org/10.5194/os-16-715-2020

Carvalho, K. S., & Wang, S. (2020). Sea surface temperature variability in the Arctic Ocean and its marginal seas in a changing climate: Patterns and mechanisms. *Global and Planetary Change*, *193*, 103265. https://doi.org/10.1016/J.GLOPLACHA.2020.103265

Casanova-Masjoan, M., Pérez-Hernáandez, M. D., Pickart, R. S., Valdimarsson, H., Ólafsdóttir, R. S., Macrander, A., et al. (2020). Along-stream, seasonal, and interannual variability of The north Iceland Irminger current and East Icelandic current around Iceland. *Journal of Geophysical Research: Oceans*, *125*(9). https://doi.org/10.1029/2020JC016283

Chafik, L. (2019). North Atlantic subpolar gyre index. In *Dataset version 3.0. Bolin Centre Database*. https://doi.org/10.17043/chafik-2019-3

Chen, W. Y., & van den Dool, H. (2003). Sensitivity of teleconnection patterns to the sign of their primary action center. *Monthly Weather Review*, *131*(11), 2885–2899. https://doi.org/10.1175/1520-0493(2003)131<2885:sotptt>2.0.co;2

Chen, X., & Tung, K. K. (2018). Global surface warming enhanced by weak Atlantic overturning circulation. *Nature*, *559*(7714), 387–391. https://doi.org/10.1038/s41586-018-0320-y

Daniault, N., Mercier, H., Lherminier, P., Sarafanov, A., Falina, A., Zunino, P., et al. (2016). The northern North Atlantic Ocean mean circulation in the early 21st century. *Progress in Oceanography*, *146*, 142–158. https://doi.org/10.1016/j.pocean.2016.06.007

Dee, D. P., Balmaseda, M., Balsamo, G., Engelen, R., Simmons, A. J., & Thépaut, J. N. (2014). Toward a consistent reanalysis of the climate system. *Bulletin of the American Meteorological Society*, *95*(8), 1235–1248. https://doi.org/10.1175/BAMS-D-13-00043.1

de Jong, M. F., & de Steur, L. (2016). Strong winter cooling over the Irminger Sea in winter 2014-2015, exceptional deep convection, and the emergence of anomalously low SST. *Geophysical Research Letters*, *43*(13), 7106–7113. https://doi.org/10.1002/2016GL069596

Desbruyères, D., Chafik, L., & Maze, G. (2021). A shift in the ocean circulation has warmed the subpolar North Atlantic Ocean since 2016. *Communications Earth & Environment*, *2*(1), 1–9. https://doi.org/10.1038/s43247-021-00120-y

Deser, C., Alexander, M. A., Xie, S.-P., & Phillips, A. S. (2010). Sea surface temperature variability: Patterns and mechanisms. *Annual Review of Marine Science*, *2*(1), 115–143. https://doi.org/10.1146/annurev-marine-120408-151453

Dickson, R. R., Osborn, T. J., Hurrell, J. W., Meincke, J., Blindheim, J., Adlandsvik, B., et al. (2000). The Arctic Ocean response to the North Atlantic oscillation. *Journal of Climate*, *13*(15), 2671–2696. https://doi.org/10.1175/1520-0442(2000)013<2671:taortt>2.0.co;2

Donlon, C. J., Martin, M., Stark, J., Roberts-Jones, J., Fiedler, E., & Wimmer, W. (2012). The operational sea surface temperature and sea ice analysis (OSTIA) system. *Remote Sensing of Environment*, *116*, 140–158. https://doi.org/10.1016/j.rse.2010.10.017

Furevik, T. (2000). On anomalous sea surface temperatures in the Nordic seas. *Journal of Climate*, *13*(5), 1044–1053. https://doi.org/10.1175/1520-0442(2000)013<1044:oassti>2.0.co;2

Good, S., Fiedler, E., Mao, C., Martin, M. J., Maycock, A., Reid, R., et al. (2020). The current configuration of the OSTIA system for operational production of foundation sea surface temperature and ice concentration analyses. *Remote Sensing*, *12*(4), 720. https://doi.org/10.3390/RS12040720

Häkkinen, S., & Rhines, P. B. (2004). Decline of subpolar North Atlantic circulation during the 1990s. *Science*, *304*(5670), 555–559. https://doi.org/10.1126/science.1094917

Häkkinen, S., Rhines, P. B., & Worthen, D. L. (2011). Warm and saline events embedded in the meridional circulation of the northern North Atlantic. *Journal of Geophysical Research: Oceans*, *116*(3), 3006. https://doi.org/10.1029/2010JC006275

Hansen, B., & Østerhus, S. (2000). North Atlantic-Nordic seas exchanges. *Progress in Oceanography*, *45*(2), 109–208. https://doi.org/10.1016/S0079-6611(99)00052-X

Hattermann, T., Isachsen, P. E., von Appen, W.-J., Albretsen, J., & Sundfjord, A. (2016). Eddy-driven recirculation of Atlantic water in Fram Strait. *Geophysical Research Letters*, *43*, 3406–3414. https://doi.org/10.1002/2016GL068323

Hátún, H., Payne, M. R., Beaugrand, G., Reid, P. C., Sandø, A. B., Drange, H., et al. (2009). Large bio-geographical shifts in the north-eastern Atlantic Ocean: From the subpolar gyre, via plankton, to blue whiting and pilot whales. *Progress in Oceanography*, *80*(3–4), 149–162. https://doi.org/10.1016/j.pocean.2009.03.001

Hátún, H., Sande, A. B., Drange, H., Hansen, B., & Valdimarsson, H. (2005). Ocean science: Influence of the Atlantic subpolar gyre on the thermohaline circulation. *Science*, *309*(5742), 1841–1844. https://doi.org/10.1126/science.1114777

Hersbach, H., Bell, B., Berrisford, P., Biavati, G., Horányi, A., Muñoz Sabater, J., et al. (2018). ERA5 hourly data on single levels from 1979 to present. Copernicus climate change Service (C3S) Climate Data Store (CDS). https://doi.org/10.24381/cds.adbb2d47

Holliday, N. P., Hughes, S. L., Bacon, S., Beszczynska-Möller, A., Hansen, B., Lavín, A., et al. (2008). Reversal of the 1960s to 1990s freshening trend in the Northeast North Atlantic and Nordic seas. *Geophysical Research Letters*, *35*(3). https://doi.org/10.1029/2007GL032675

Hurrell, J. W. (1995). Decadal trends in The north Atlantic oscillation: Regional temperatures and precipitation. *Science*, *269*(5224), 676–679. https://doi.org/10.1126/SCIENCE.269.5224.676

Jeansson, E., Olsen, A., & Jutterström, S. (2017). Arctic intermediate water in the Nordic seas, 1991–2009. *Deep-Sea Research Part I Oceanographic Research Papers*, *128*, 82–97. https://doi.org/10.1016/j.dsr.2017.08.013

Jónsson, S., & Valdimarsson, H. (2012). Water mass transport variability to the North Icelandic shelf, 1994-2010. *ICES Journal of Marine Science*, *69*(5), 809–815. https://doi.org/10.1093/icesjms/fss024

Kenigson, J. S., & Timmermans, M. L. (2021). Nordic seas hydrography in the context of arctic and North Atlantic Ocean dynamics. *Journal of Physical Oceanography*, *51*(1), 101–114. https://doi.org/10.1175/JPO-D-20-0071.1

Lentz, S. J., & Largier, J. (2006). The influence of wind forcing on the Chesapeake Bay buoyant coastal current. *Journal of Physical Oceanography*, *36*(7), 1305–1316. https://doi.org/10.1175/JPO2909.1

Lozier, M. S., & Stewart, N. M. (2008). On the temporally varying northward penetration of mediterranean overflow water and eastward penetration of Labrador Sea water. *Journal of Physical Oceanography*, *38*(9), 2097–2103. https://doi.org/10.1175/2008JPO3908.1

Masson-Delmotte, V., Zhai, P., Pörtner, H.-O., Roberts, D., Skea, J., Shukla, P. R., et al. (2019). Global warming of 1.5°C an IPCC Special Report on the impacts of global warming of 1.5°C above pre-industrial levels and related global greenhouse gas emission pathways, in the context of strengthening the global response to the threat of climate change, sustainable development, and efforts to eradicate poverty. In *Science officer science assistant graphics officer working group I technical support unit*. In *Nature* (Vol. 291). https://doi.org/10.1038/291285a0.5813

Meredith, M., & Martin, S. (2019). Polar regions. In: *IPCC special report on the ocean and cryosphere in a changing climate* [In H.-O. Pörtner, D. C. Roberts, V. Masson-Delmotte, P. Zhai, M. Tignor, E. Poloczanska (Eds.), et al. Retrieved from https://www.ipcc.ch/srocc/chapter/chapter-3-2/citation/

Mikhailova, N. v., Bayankina, T. M., & Sizov, A. A. (2021). Two modes of atmosphere–ocean interaction in the Atlantic sector of the Arctic Basin. *Oceanology*, *61*(4), 443–449. https://doi.org/10.1134/S0001437021030097

Orvik, K. A., & Niiler, P. (2002). Major pathways of Atlantic water in the northern North Atlantic and Nordic seas toward Arctic. *Geophysical Research Letters*, *29*(19), 2–1. https://doi.org/10.1029/2002GL015002

Østerhus, S., Woodgate, R., Valdimarsson, H., Turrell, B., de Steur, L., Quadfasel, D., et al. (2019). Arctic Mediterranean exchanges: A consistent volume budget and trends in transports from two decades of observations. *Ocean Science*, *15*(2), 379–399. https://doi.org/10.5194/OS-15-379-2019

Raj, R. P., Chatterjee, S., Bertino, L., Turiel, A., & Portabella, M. (2019). The Arctic front and its variability in the Norwegian Sea. *Ocean Science*, *15*(6), 1729–1744. https://doi.org/10.5194/OS-15-1729-2019

Sandø, A. B., Nilsen, J. E. Ø., & Bentsen, M. (2012). Mechanisms for variable North Atlantic-Nordic seas exchanges. *Journal of Geophysical Research: Oceans*, *117*(12). https://doi.org/10.1029/2012JC008177

Sarafanov, A. (2009). On the effect of the north Atlantic oscillation on temperature and salinity of the subpolar north Atlantic intermediate and deep waters. *ICES Journal of Marine Science*, *66*(7), 1448–1454. https://doi.org/10.1093/ICESJMS/FSP094

Serreze, M. C., Barrett, A. P., Slater, A. G., Steele, M., Zhang, J., & Trenberth, K. E. (2007). The large-scale energy budget of the Arctic. *Journal of Geophysical Research Atmospheres*, *112*(11). https://doi.org/10.1029/2006JD008230

Smedsrud, L. H., Muilwijk, M., Brakstad, A., Madonna, E., Lauvset, S. K., Spensberger, C., et al. (2022). Nordic seas heat loss, Atlantic inflow, and Arctic Sea Ice cover over the last century. *Reviews of Geophysics*, *60*(1), e2020RG000725. https://doi.org/10.1029/2020RG000725

Somavilla, R., González-Pola, C., & Fernández-Diaz, J. (2017). The warmer the ocean surface, the shallower the mixed layer. How much of this is true? *Journal of Geophysical Research: Oceans*, *122*(9), 7698–7716. https://doi.org/10.1002/2017JC013125

Stark, J. D., Donlon, C. J., Martin, M. J., & McCulloch, M. E. (2007). OSTIA: An operational, high resolution, real time, global sea surface temperature analysis system. In *OSTIA: An operational, high resolution, real time, global sea surface temperature analysis system. OCEANS 2007 - Europe*. https://doi.org/10.1109/OCEANSE.2007.4302251

Sutherland, D. A., & Pickart, R. S. (2008). The East Greenland coastal current: Structure, variability, and forcing. *Progress in Oceanography*, *78*(1), 58–77. https://doi.org/10.1016/j.pocean.2007.09.006

Tsubouchi, T., Våge, K., Hansen, B., Larsen, K. M. H., Østerhus, S., Johnson, C., et al. (2021). Increased ocean heat transport into the Nordic seas and Arctic Ocean over the period 1993–2016. *Nature Climate Change*, *11*(1), 21–26. https://doi.org/10.1038/s41558-020-00941-3

van den Dool, H. M., Saha, S., & Johansson, Å. (2000). Empirical orthogonal teleconnections. *Journal of Climate*, *13*(8), 1421–1435. https://doi.org/10.1175/1520-0442(2000)013<1421:eot>2.0.co;2

Visbeck, M., Chassignet, E. P., Curry, R. G., Delworth, T. L., Dickson, R. R., & Krahmann, G. (2003). The ocean's response to North Atlantic oscillation variability. *Geophysical Monograph Series*, *134*, 113–145. https://doi.org/10.1029/134GM06

Zhao, J., Yang, S., Semper, S. A., Pickart, R. S., Våge, K., Valdimarsson, H., & Jónsson, S. (2018). Numerical study of interannual variability in The north Iceland Irminger current. *Journal of Geophysical Research: Oceans*, *123*(12), 8994–9009. https://doi.org/10.1029/2018jc013800